Bulletin of the New Zealand Society for Earthquake Engineering, Vol. 55, No. 2, June 2022

EXPERIMENTAL AND NUMERICAL ANALYSIS OF THE LATERAL RESPONSE OF FULL-SCALE BRIDGE PIERS

Pavan Chigullapally[1], Lucas S. Hogan[2], Liam M. Wotherspoon[3], Max Stephens[4] and Michael J. Pender[5]

(Submitted *May 2021*; Reviewed *August 2021*; Accepted *September 2021*)

ABSTRACT

This paper presents the results of in-situ testing of two integrated pile-columns of a partially demolished bridge located in Auckland, New Zealand. A series of tests involving lateral monotonic pushover and subsequent dynamic free vibration snapback tests were used to quantify the variation in the stiffness and damping behaviour of the pile-column specimens over a range of lateral load levels. Each testing sequence consisted of incrementally increasing peak monotonic loads followed by the dynamic snapback, with a series of varying peak loads at the end of the testing sequence to evaluate the influence of loading history on the monotonic and dynamic response. The secant stiffness between the monotonic pushover tests performed to the same loading levels before and after the maximum load was applied, reduced by up to 40% in both the pile-columns, primarily due to soil gapping effects, highlighting the significant potential softening of the system prior to pile or column yielding. Progressive reduction in the damping of the system during each snapback test was evident, due to the varying contributions of different energy dissipation mechanisms, and the level of damping varied depending on the peak load applied. These results highlighted the significant influence of soil gapping and nonlinearity on the dynamic response of the system. Numerical models were developed in the open source structural analysis software OpenSeesPy using a Nonlinear Beam on Winkler Foundation approach to further investigate the response of the pile-columns. Models of both the pile-columns using existing p-y curves for clay soils showed good agreement with the experimental data in load-displacement, period and snapback acceleration time histories. Sensitivity analysis showed that the surface soft clay layer had a significant effect on the lateral response and dynamic characteristics of the model, reinforcing the need for good characterisation of the near surface soil profile to capture the behaviour of the system.

INTRODUCTION

The importance of accounting for soil-foundation-structure interaction (SFSI) in the seismic response of bridges has been widely acknowledged for many years [1-5]. An important part of the assessment of SFSI effects is the definition of the stiffness and damping characteristics of foundations. One of the inherent difficulties in accounting for these effects, particularly in a design setting, is this small number of large-scale pile foundations tests that have been performed relative to the wide range of structural and geotechnical characteristics that can be encountered in practice. This limitation means that there is often insufficient field test data to constrain the nonlinear stiffness and damping behaviour of the numerical models used to design and analyse pile foundations and wider bridge structures.

The lateral response of pile foundations has been previously studied using a range of different loading methodologies. The most widely used approach is static or pushover loading, where a gradually increasing load is applied to the pile head or at a location above the ground surface on an extension of the pile shaft. Using this approach, the load can be applied either monotonically or cyclically, with both methods typically applying loads of progressively larger magnitudes. Static loading of piles of various cross-sectional characteristics have been investigated in clay soils by Matlock [6] , Kramer [7], Rollins et al. [8], Gerber and Rollins [9], Sritharan et al. [10] and Sa'don [11], in sands by Chik et al. [12], Nasr [13], Madhusudan Reddy and Ayothiraman [14], Khari et al. [15], Abadie [16] and Aguirre et al. [17], in silts by Kramer [7] and Lalicata et al. [18], and in multi-layered profiles by Rollins et al. [19], Snyder [20] and Stewart et al. [21].

To capture the effects of damping in pile foundations, dynamic loading is required. In prior studies which have implemented dynamic loading, a range of excitations of increasing magnitude have been applied using an eccentric mass shaker, hydraulic actuator, or by quick release of the load at the end of a pushover loading cycle. Dynamic loading of piles of various cross-sectional characteristics have been investigated in clay soils by Blaney and O'Neill [22], Crouse et al. [23], Boominathan [24], Sa'don et al. [25] and Fleming et al. [26], in sands by Scott et al. [27], Ting [28], Chai and Hutchinson [29], Boulanger et al. [30], Boominathan [24] and Chang and Hutchinson [31], in silts by Scott et al. [27], Ting [28], Boominathan [24], and in multi-layered profiles by Boulanger et al. [32] and Boominathan [24].

Statnamic loading is another common testing method, where the duration of the load from the statnamic device is longer than a dynamic loading test and shorter than a static loading test, characterising a response that is somewhere between static and dynamic behaviour [33,34]. Statnamic loading of piles of various cross-sectional characteristics have been investigated in clayey soils by Brown [33,35], Brown et al. [36] and Brown and Hyde [37], in sands by Brown [33], El Naggar [34] and Tobita et al. [38], in silts by Brown [33], Brown et al. [39] and Tobita et al. [38], and in multi-layered profiles by Brown et al. [39], Bowles [40] and Broderick [41].

[1] *Corresponding Author, PhD Candidate, The University of Auckland, Auckland, New Zealand, pchi893@aucklanduni.ac.nz (Member).*
[2] *Lecturer, The University of Auckland, Auckland, New Zealand, lucas.hogan@auckland.ac.nz (Member)*
[3] *Associate Professor, The University of Auckland, Auckland, New Zealand, l.wotherspoon@auckland.ac.nz (Fellow)*
[4] *Lecturer, The University of Auckland, Auckland, New Zealand, max.stephens@auckland.ac.nz (Member)*
[5] *Professor, The University of Auckland, Auckland, New Zealand, m.pender@auckland.ac.nz (Fellow)*

In general, the outcomes from previous research have provided designers with improved estimates of dynamic lateral stiffness and damping of pile foundations in several types of soil profiles along the depth of pile. Previous testing has enabled the development, evaluation and improvement of static and dynamic p-y curves for non-linear models and improved the existing theoretical equations for estimating SFSI effects. However, even with the significant number of large-scale pile tests in existing literature, there are few tests in soil profiles with soft surface layers underlain by much stiffer soils, as can often be found in the alluvial conditions at bridge river crossings. Due to the limited amount of in-situ test data, the design of piles in these soil conditions usually ignores the top soft layers if they are in locations prone to scour [42].

This paper presents the results of in-situ testing of integrated pile-columns of a partially demolished bridge located in Auckland, New Zealand. A test sequence involving static pushover and dynamic free vibration snapback tests was used to capture the change in dynamic response, stiffness and damping of the system due to pile cracking, soil gapping and soil nonlinearity. The characteristics of the bridge and the field-testing methodology are first presented, and the field testing results are discussed. To further explore the results from the field testing, a numerical model of each specimen was developed using the open-source structural analysis software OpenSeesPy [43]. Modelling results are compared to the field response and the sensitivity of key parameters controlling the response of the integrated pile-columns are evaluated and discussed.

FIELD TESTING SETUP AND METHODOLOGY

To investigate the performance of in-service bridge foundations, an experimental program was undertaken at Henderson Creek in Auckland, New Zealand. The Henderson Creek site consisted of two separate five span, reinforced concrete bridges that traverse a tidal creek, with this study focussing on Henderson Creek Bridge No. 2. This bridge was constructed in 1962, with an overall length of 93 m and a width of 9.35 m that supported two lanes of traffic. The superstructure of the bridge was supported by piers consisting of four 990 mm diameter reinforced concrete extended pile-columns with a centre to centre spacing of 2.24 m, connected by a 1.8 m x 1.09 m pier cap (Figure 1). The above and below ground sections of the extended pile-columns had the same diameter, with the pile extending to a depth of 15.1 m, and no pile cap at the ground surface. The reinforcing steel layout is summarised in Figure 2 and consisted of twenty-four D32 longitudinal bars (32 mm diameter, f_y = 300 MPa) and a spiral transverse reinforcement of 19 mm diameter (f_y = 300 MPa) at 114 mm c/c. On the day of testing, the ground level was 6.55 m below the top of pile cap and water was present above the ground level during the testing.

The field testing programme focussed on the response of two of the extended pile-columns from one of the piers, referred to herein as Specimen 1 and Specimen 2. To isolate the test specimens the bridge deck and the longitudinal beams were removed, then the pile-columns were isolated by saw cutting through the pier cap at the locations shown in Figure 1, creating a clear gap of 1 m to prevent any interaction between the Specimens and other parts of the pier during testing.

The soil profile at the testing locations were characterised using a set of cone penetration tests (CPT) and rotary boreholes with Standard Penetration Tests (SPT). A total of four boreholes and eleven CPTs were used to characterise the soil profile at the test locations. These profiles are summarised in Figure 2. At the location of Specimen 1, a 4.5 m thick layer of soft alluvium was present at the ground surface, with a CPT tip resistance (q_c) of 0.6 MPa and SPT N_{60} values of 2-8. Beneath this surface layer was a 1.5 m layer of highly-to-moderately-weathered East Coast Bays Formation (ECBF) sandstone and siltstone with a q_c of 6 MPa throughout the layer. At the location of Specimen 2, an 8.1 m thick layer of soft alluvium was present at the ground surface, with q_c of 0.4 MPa and SPT N_{60} values of 2-8. This surface layer was underlain by a 3 m layer of highly-to-moderately-weathered ECBF with q_c of 5 MPa throughout the layer. The lower stratum for both Specimen 1 and Specimen 2 was slightly weathered ECBF with q_c of 30 MPa, transitioning to unweathered ECBF over a depth of a few metres, with CPT refusal at this point. This unweathered ECBF formed the bearing layer for each specimen.

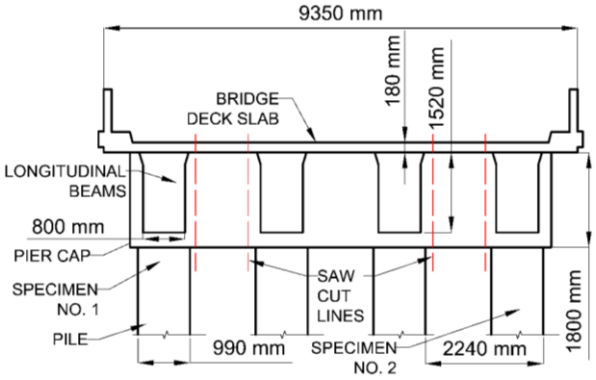

Figure 1: Section view of the Henderson Creek Bridge pier dimensions, including the location of saw cuts used to separate each extended pile-column for testing.

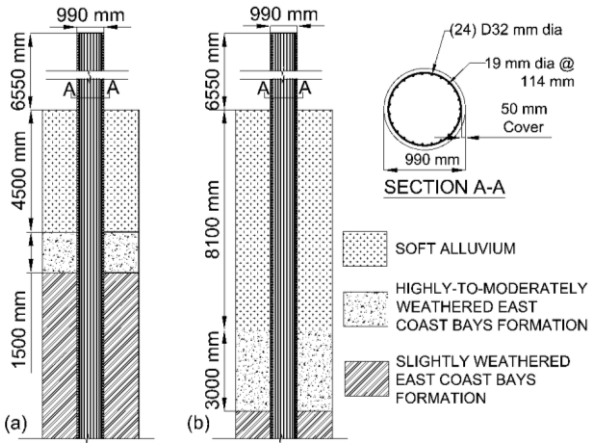

Figure 2: Soil profile characteristics, pile-column dimensions and pile-column cross sectional details for: (a) Specimen 1; and (b) Specimen 2.

Testing Sequence

Testing was conducted to capture the change in dynamic response, stiffness and damping of the specimens. The testing of each specimen was performed in two parts: 1) a monotonic pushover (referred to as pushover herein) in which a horizontal load was applied slowly until a target load was reached and 2) a snapback in which the horizontal load was released at the target load, allowing the specimen to undergo free vibration. Table 1 summarises the loading sequence applied to each test specimen. A similar loading sequence was applied for both specimens, with a gradual increase in the target load up to Test 5, followed by a sequence of fluctuating target loads to assess the effect of past loading on the response.

Testing Methodology

The lateral load was applied to the top of each specimen using two pre-stressing strands that extended between steel loading

frames attached to the top of the specimen and to the longitudinally adjacent bridge pier as shown in Figure 3 and Figure 4, similar to those used in bridge pier testing by Wood and Phillips [44]. The pier cap of the adjacent bridge pier was unaltered and acted as a reaction pier during testing. Each loading frame was hooked behind the back of the specimens and the reaction pier and secured with concrete anchors. Lateral load was applied 6.55 m above the ground level using a hydraulic actuator attached to the pre-stressing strands. The actuator was located inside the loading frame on the reaction pier and pushed a sliding block within the loading frames to tension the pre-stressing strands, as shown in Figure 4. The pre-stressing strands were installed with an initial slack to allow unrestrained movement of the specimens during free vibration. An electric pump was used to perform the static pushover test, increasing the horizontal load up to the target level for each pushover test. At the end of each pushover test, a snapback test was performed by dumping the hydraulic fluid from the actuator into a reservoir by remotely triggering a solenoid valve, creating a sudden release of load and allowing free vibration response.

Instrumentation

To measure the force-displacement response of the specimen during pushover testing, a Linear Variable Differential Transformer (LVDT) was positioned at the top of the specimen and connected to a reference frame supported by the adjacent pile. A load cell was connected to the actuator inside the loading frame at the reaction pier. To measure the dynamic response of the specimen during snapback testing, accelerometers were placed along the height of the specimen as indicated in Figure 3. An additional accelerometer was installed at the top of specimen in the direction perpendicular the loading direction to capture any out-of-plane accelerations. Throughout the duration of testing, the water level varied by up to a metre above the ground level, so it was not feasible to provide instrumentation near the ground surface.

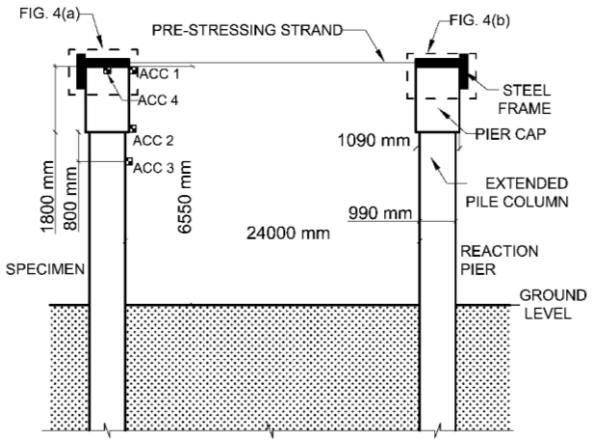

Figure 3: Schematic of the test setup with loading frames and accelerometers (ACC) attached to the specimen and the reaction pier (not to scale).

Table 1: Test sequence for each specimen and the maximum load applied in each pushover test.

		Test 1	Test 2	Test 3	Test 4	Test 5	Test 6	Test 7	Test 8	Test 9
Specimen 1	Load (kN)	47	51	97	142	166	50	148	97	48
	Test ID	S1_T1	S1_T2	S1_T3	S1_T4	S1_T5	S1_T6	S1_T7	S1_T8	S1_T9
Specimen 2	Load (kN)	52	52	98	149	150	48	103	101	50
	Test ID	S2_T1	S2_T2	S2_T3	S2_T4	S2_T5	S2_T6	S2_T7	S2_T8	S2_T9

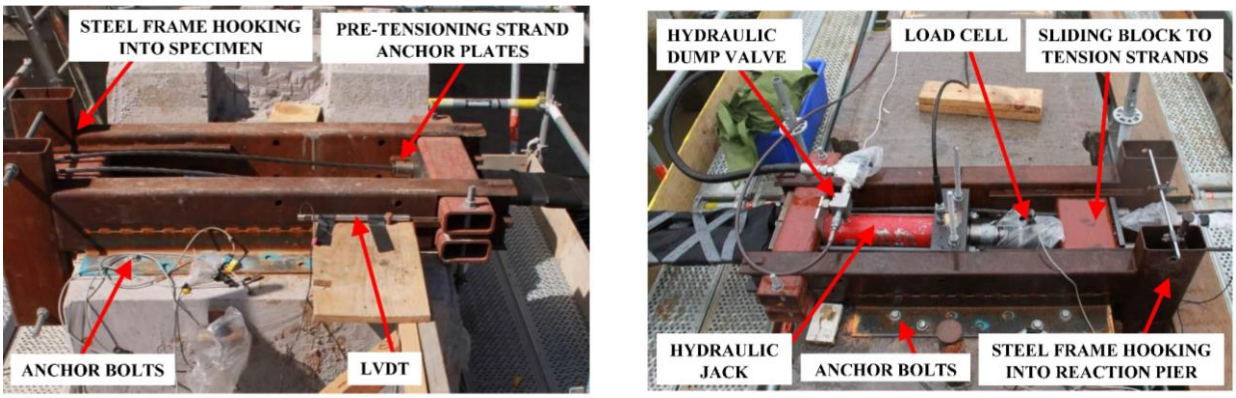

(a) (b)

Figure 4: Details of the test equipment layout with: (a) Load frame attached to the specimen; (b) Load frame and actuator attached to the reaction pier.

FIELD TESTING OBSERVATIONS

Static Pushover Testing

During the static pushover testing, specimens were pushed into the soil, and this resulted in plastic deformation on one side of the pile and opening of a gap on the other side as there was a separation between the pile and soil. At the end of a loading cycle when the load was released, there was a gap in front of the pile due to the plastic deformation of the soil, which along with the gap behind the pile reduced the stiffness of the system. This can be seen in the load-displacement response for Specimen 1 and Specimen 2 are shown in Figure 5. The load-displacement response for Specimen 1 is shown in Figure 5 (a) with the drift between the top of the pile and the ground level. Specimen 1 remained elastic during the first two low level pushover tests. A slight change in the secant stiffness was observed during S1_T3 at approximately 50 kN when the cracking moment of the pile section (M_{cr} = 310 kN-m) was exceeded in the critical sections of the specimen. At the start of S1_T5, there was a residual displacement of approximately 8 mm at the top of the specimen. This residual displacement can be attributed to: (1) small residual rotations at and below the ground level due to incomplete closure of cracks and the low axial load on the specimen [45]; (2) soil plastic deformation and the development of a gap between the pile and the surrounding soil during the previous pushover and snapback tests. While the gapping could not be observed directly due to the water level of the river, the load-displacement response in S1_T5 shows signs of gapping similar to other large scale pile test studies [1,26]. Namely, the secant stiffness at the beginning of the monotonic push was lower than the previous tests due to the loss of contact with the surrounding soil, and as the gap closed it put the pile in contact with a larger area of soil, increasing the stiffness of the system. After the gap fully closed, the S1_T5 curve aligned with the backbone curve from S1_T4. A similar behaviour of increasing secant stiffness at the later stages of the static pushover loading was observed in S1_T7. The load-displacement response of the specimen after S1_T5 remained linear, as all subsequent load levels following S1_T5 were less than the maximum load achieved in S1_T5, meaning it is unlikely additional gapping or soil nonlinearity developed.

The load-displacement response of Specimen 2 is shown in Figure 5 (b). The specimen response was elastic up to a load of approximately 30 kN during S2_T1. At the start of S2_T4 there was some residual displacement that developed through the same mechanisms described for Specimen 1 previously, and the load-displacement response was similar to that observed for Specimen 1 in S1_T5. A similar behaviour of increasing secant stiffness during gap closing was also observed in S2_T5. The load-displacement response of the specimen after S2_T5 remained linear as the load levels were less than the maximum load applied in S2_T5 and are similar to the response in the same tests in Specimen 1, except that 5 mm of additional residual deformation was observed following S2_T5. Note that Specimen 2 exhibited approximately half the stiffness of Specimen 1 during Tests 1-4 as well as larger residual displacement following Tests 4-6. These phenomena are likely due to more extensive cracking of the pile section prior to the start of testing and lower strength and stiffness of the soil layers at the location of Specimen 2 respectively.

Even though the load levels in Test 3 were twice that of Test 6 for both specimens, the peak displacements were very similar. This is a clear demonstration of the influence of gap formation between the pile and surrounding soil, reducing the overall stiffness of the specimen. For both the 100 kN tests (Test 3 and Test 8) there was a reduction in the secant stiffness of approximately 40%. The reduction in secant stiffness can be attributed to both an increase in soil gapping around the specimen and an increase in cracking of the pile section after the maximum target load was reached in Test 4 and Test 5. During the testing of both the specimens, the peak load levels were not large enough to exceed the yield bending moment of 1630 kN-m. The maximum load levels during the testing sequence were representative of the serviceability limit state design loads for this bridge.

Snapback Testing

Following the monotonic push to each target load in Table 1, a snapback test was performed to determine the dynamic properties of the specimens. The free vibration response of snapback tests for Specimen 1 and Specimen 2 are shown in Figure 6 and Figure 7 respectively. A summary of all the snapback test results is provided in an electronic supplement to allow for brevity here.

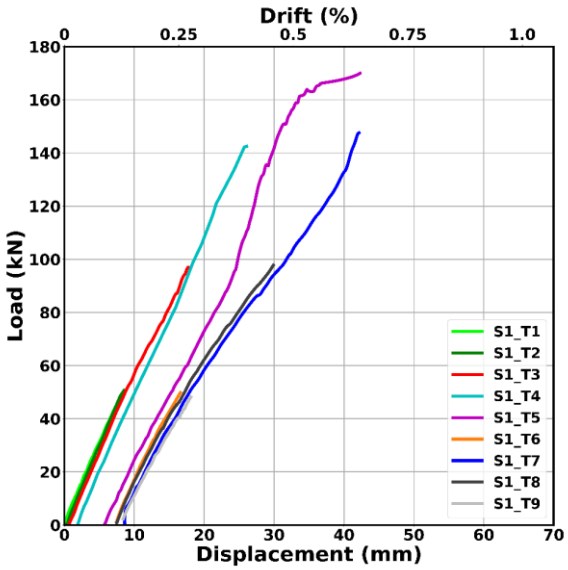

(a)

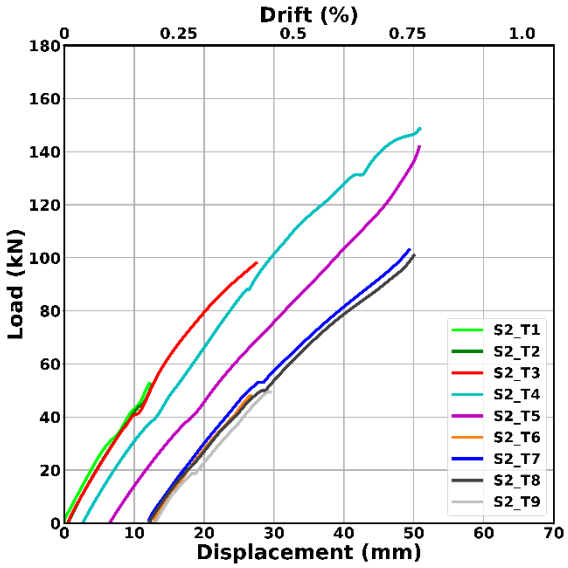

(b)

Figure 5: Summary of the load-displacement behaviour of test specimens during static pushover loading for all target loads: a) Specimen 1; b) Specimen 2.

For both specimens, the peak to peak amplitude decay during free vibration occurred at a relatively slow rate for tests with release loads lower than 100 kN (as illustrated by Figures 6a and 6d, and 7a and 7d). In contrast, tests with release loads greater than 100 kN displayed a free vibration response with two distinct stages. Initially, there was a large reduction in amplitude during the first one to two cycles, which was followed by subsequent decay rates similar to that of the tests with lower initial release loads (as illustrated by Figures 6b and 6c, and 7b and 7c).

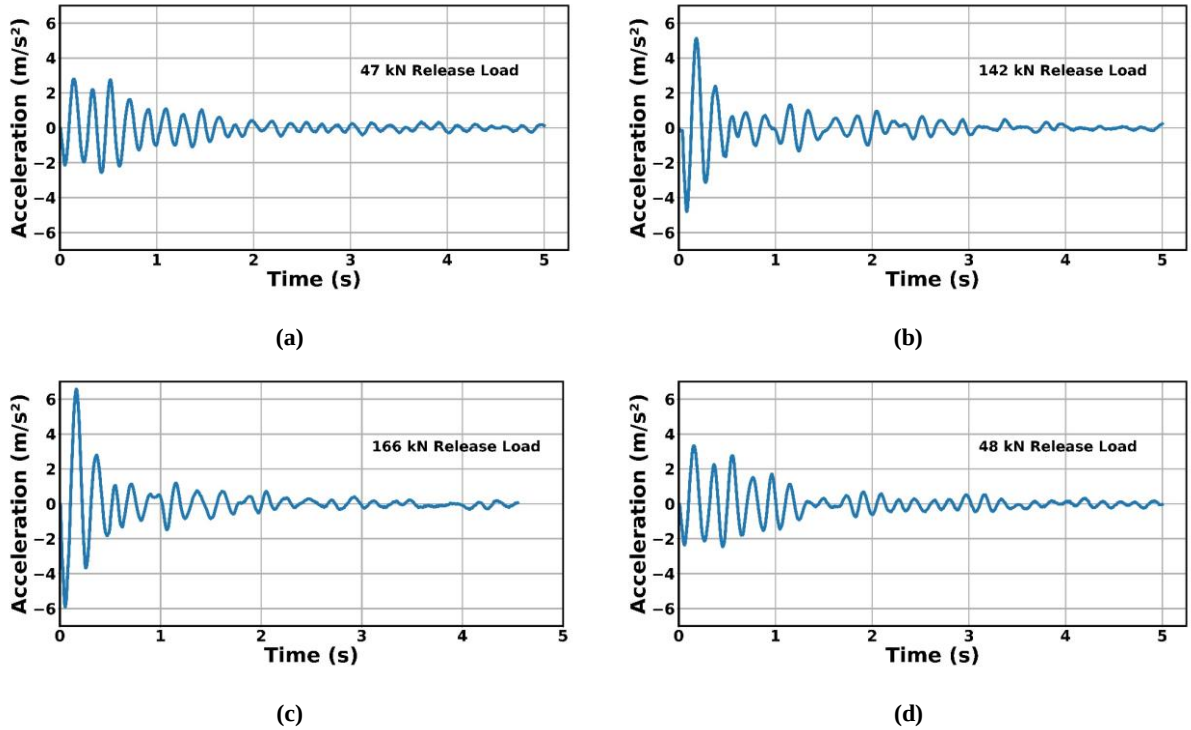

Figure 6: Acceleration time histories of Specimen 1 during snapback testing: (a) S1_T1; (b) S1_T4; (c) S1_T5; (d) S1_T9.

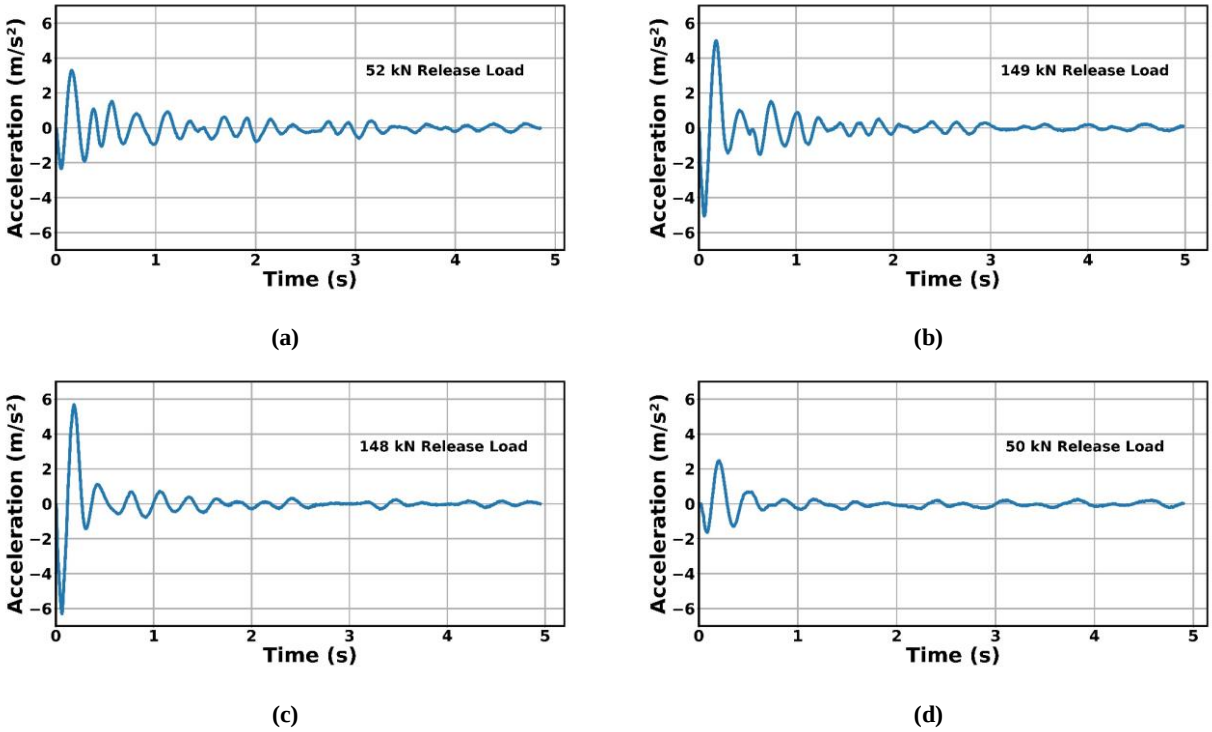

Figure 7: Acceleration time histories at the top of Specimen 2 during snapback testing: (a) S2_T1; (b) S2_T4; (c) S2_T5; (d) S2_T9.

The natural period of the two specimens was estimated for each snapback test using a combination of peak picking from Fast Fourier Transformation (FFT) and peak to peak intervals from the time series data. The resulting natural periods for each specimen are summarised in Figure 8. The range of natural period varied from 0.19 s to 0.24 s for Specimen 1 and 0.2 s to 0.29 s for Specimen 2. The natural period for Specimen 1 increased from 0.19 s to 0.22 s between tests S1_T1 and S1_T5 and then reduced to 0.2 s in S1_T9. Similarly, the natural period for Specimen 2 increased from 0.2 s to 0.29 s between test S2_T1 and S2_T5, and then reduced to 0.265 s in S2_T9. The natural period for both specimens increased as the peak load increased until the maximum peak load in Test 5, and then reduced with a reduction in peak load in subsequent tests. The natural periods were higher in tests after maximum peak load application compared to the same load levels before the application of the maximum peak load application in Test 5. This variation in natural period can be attributed to an increase in the formation of a gap between specimen and surrounding soil and specimen cracking. Tests with release loads above 100 kN had a 5% increase in the natural period between the initial rapid amplitude decay and the slow amplitude decay in later stages of the test. The range of natural periods for Specimen 2 were larger than the range of natural periods for Specimen 1 due to more significant cracking in the pile section in Specimen 2 prior to the start of testing and the lower strength and stiffness of soil layers surrounding Specimen 2.

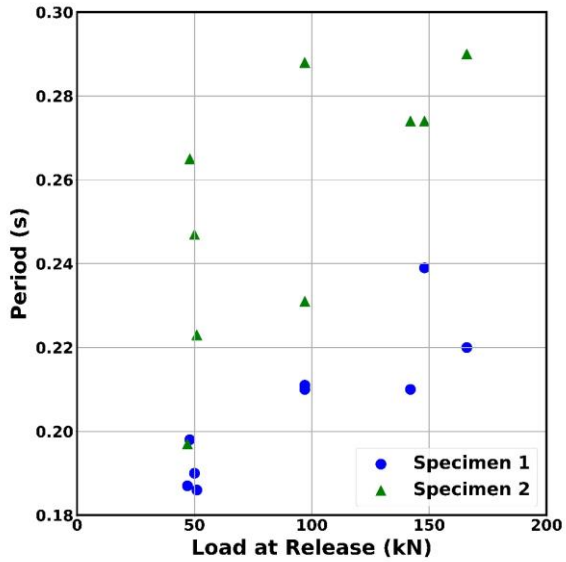

Figure 8: Variation of the natural period for Specimen 1 and Specimen 2 with respect to the maximum load at release for each test.

The time series data in Figure 6 and Figure 7 indicate that damping was not consistent throughout the duration of the free vibration, being influenced by a combined mechanism including the impact between the pile and the surrounding soil and soil gapping around the pile. The contribution of each component to the total damping depends on the magnitude of the snapback release load and this contribution changes as the number of cycles of vibration increases.

To assess the variation in damping of each specimen throughout the response histories, equivalent viscous damping was determined using the logarithmic decrement method [46]. Multiple damping values were calculated from each test using sets of acceleration peaks from several stages of the response histories. This enabled a simplified equivalent viscous damping representation of the complex damping contributions from the previously discussed phenomena. The calculated equivalent viscous damping values are plotted in Figure 9 as a function of acceleration. The range of the maximum equivalent viscous damping estimates across all tests varied from 3.3% to 15% for Specimen 1 and 6% to 25% for Specimen 2. The maximum damping for Specimen 1 increased from 3.3% to 14% from S1_T1 to S1_T5 and then reduced to 6% in S1_T9. Similarly, the damping for Specimen 2 increased from 6% to 25% from S2_T1 to S2_T5, then reduced to 17% in S2_T9. This shows that the equivalent viscous damping values of 10% and 15% suggested by the New Zealand Transport Agency [47] for pier piles in granular and sandy soils and clay soils respectively provide a conservative estimate of the damping these components provide. Changes in the specimen properties meant that there was an increase in damping from the start to the end of the test sequence. The higher initial damping at low load levels in Specimen 2 compared to Specimen 1 could be due to the different soil profile characteristics and/or cracking of Specimen 2 prior to the start of testing.

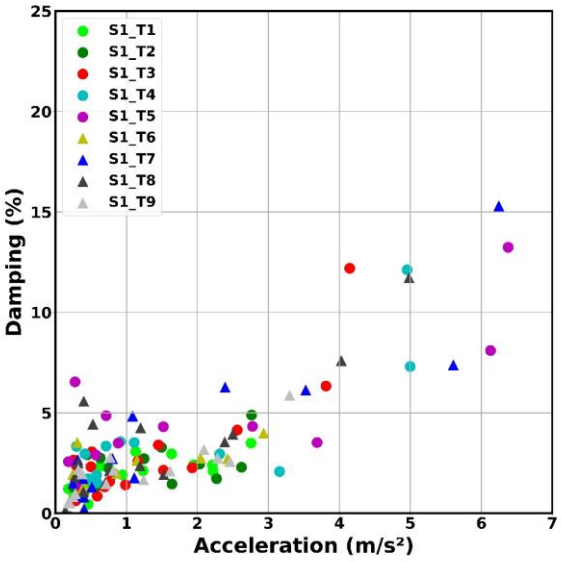

(a)

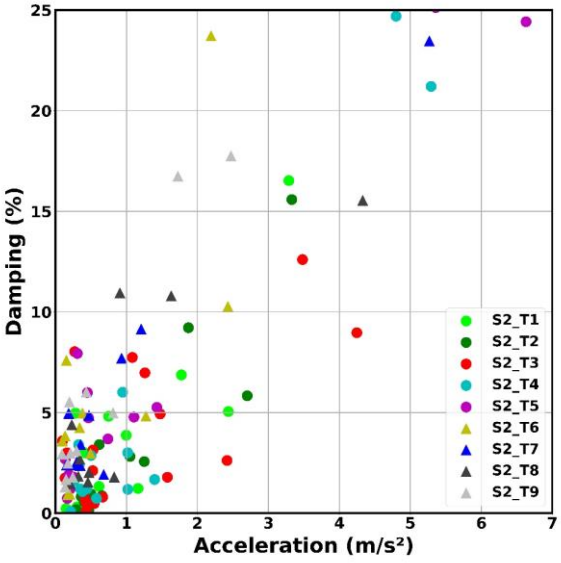

(b)

Figure 9: Variation of equivalent viscous damping with respect to acceleration using the free vibration response of (a) Specimen 1; (b) Specimen 2.

From Figure 9, it is clear there is a relationship between acceleration and the calculated equivalent viscous damping value. The maximum equivalent viscous damping in both specimens increased as the initial acceleration levels increased. The damping in subsequent tests were lower than the maximum viscous damping calculated for Test 5 but were higher than damping calculated for equivalent loads in tests conducted prior to Test 5. The high initial equivalent viscous damping for higher initial accelerations can be attributed to the dissipation of energy through the impact between the pile and the surrounding soil which occurs during the first half cycle of the free vibration response. The high initial equivalent viscous damping values would increase further when the specimen is pushed closer to the design level event demands. After this first half-cycle, the gap formation between the pile and soil influences the level of radiation damping of the foundation system. With the multiple mechanisms of energy dissipation that vary throughout the test and influence damping, it is not possible to represent damping throughout the entire response history using a single value of equivalent viscous damping. These variations in equivalent viscous damping were consistent with the observations made by other researchers [11,23].

FINITE ELEMENT MODELLING OF TEST BEHAVIOUR

The experimental results were used to validate numerical modelling procedures for integrated pile-columns using a Nonlinear Beam on Winkler Foundation approach. The open-source structural analysis program OpenSeesPy [43] was used to simulate the monotonic and dynamic snapback response of the integrated pile-columns tested in the experimental program whilst accounting for material and soil nonlinearity. This model calibration included the comparison of OpenSeesPy models with field tests in lateral load-displacements at the top of specimens during static pushover tests, the acceleration time histories at the top of specimens, and the variation in natural period of the specimen-soil system during free vibration. The validated numerical modelling procedures were then used to perform a sensitivity analysis study to identify the key parameters controlling the monotonic and dynamic response of the pile columns.

Model Overview

The integrated pile column models were modelled using displacement based distributed plasticity beam-column elements with three integration points. The column (above the ground level) was discretised into 40 equal length elements while the pile (below the ground level) was divided into 71 elements with smaller elements near the ground surface to capture the behaviour in the active pile length region. A convergence study was used to determine the number of elements within the column, as the natural period was sensitive to the number of elements above ground level. Mass corresponding to the tributary length of the pile-column cross section was lumped at the nodes between elements using a concrete density of 2400 kg/m3. An additional mass of 200 kg was lumped at the top of the column to account for test equipment. No P-delta effects were considered in the modelling as the peak drifts experienced during field testing were less than 1% and no additional axial load was applied to the test specimens.

Lateral loads were applied to the top of the column as static pushover loads. Force controlled loading was used to load all the specimens at the top of the specimen to replicate the field test loading conditions. All tests were modelled sequentially to ensure residual deformations in the system were captured. The snapback tests were modelled by releasing the lateral load and allowing free vibration. The rate of loading during all the tests was kept constant and the maximum load applied at the end of each cycle matched those summarised in Table 1.

Rayleigh damping was varied between different snapback tests, and within each snapback test based on the acceleration levels, to replicate the variation in damping observed in the field testing. Higher Rayleigh damping was used in the initial stages of each test to represent the damping when impact effects were dominant, and lower Rayleigh damping was used in the final stages of each test when radiation damping was dominant. During the testing, there was less than 0.1 m of free water above the ground level, such that any contribution to damping from the influence of the water surrounding the pile was likely to be negligible. The range of the initial damping estimates across all tests varied from 3.3% at initial accelerations of 2.8 m/s^2, up to 25% for initial accelerations of 6.2 m/s^2. Damping reduced down to 1% during the later stages of free vibration when the accelerations were below 0.5 m/s^2. The target frequency used for defining the Rayleigh damping parameters were the natural frequency and three times the natural frequency for all tests. The Rayleigh damping provided to the system here was in addition to the hysteretic damping from soil and structural nonlinearity.

Pile-Column Modelling

The nonlinear behaviour of the pile-column was modelled using a fibre based approach with displacement based distributed plasticity beam-column elements. A convergence study was used to define the appropriate discretization of the fibre meshing, as it controlled the deflection of the pile-column post cracking. For every pile-column section, the core concrete fibre area was divided into 50 radial divisions and into 12 circumferential divisions, and the cover concrete area was divided into 20 radial division and 16 circumferential divisions.

Table 2: Concrete material properties used in OpenSeesPy modelling for different regions of a section.

Region	f'c (MPa)	Peak Strain	Tensile Strength (MPa)
Unconfined	52.5	0.0028	5.3
Confined	61.5	0.0052	5.3
Cracked	52.5	0.0028	0

Unconfined and confined concrete fibres were modelled using the Kent-Scott-Park material model with linear tension stiffening (Concrete02 in OpenSeespy). Steel reinforcement fibres were modelled using a bilinear material model with kinematic hardening (Steel01 in OpenSeespy) with a yield strength of 300 MPa and strain hardening ratio of 0.01. The properties for each concrete material model are summarised in Table 2. Unconfined compressive strength was modified to account for ageing effects [48] and confined concrete properties were defined using the Mander et al. [49] model. For Specimen 1, uncracked concrete sections were considered for the entire length of specimen. Based on the pushover test results, Specimen 2 had a lower initial stiffness which was attributed to initial cracking. To represent the effect of the reduced stiffness in the model, cracked concrete sections were considered in the pile active length region, which was up to 3m below the ground surface [50], as this region was most likely to have been cracked during the service life of the specimen. The reduced stiffness values were based on Paulay and Priestley`s recommendations for cracked concrete sections [2]. In this region, the initial cracked properties were applied to the entire

cover region along with the exterior regions of the core concrete areas to achieve the recommended reduced stiffness values. The initial cracking was incorporated by using zero tensile strength in the concrete material model.

Soil Modelling

Soil was modelled using nonlinear p-y springs in OpenSeesPy [32] and were implemented using zero length elements with cyclic load-displacement relationships. The non-linear behaviour of the p-y spring is modelled using elastic, plastic and gap components in series. The gap component consists of a non-linear closure spring in parallel with non-linear drag spring as shown in Figure 10. The p-y soil springs for soft alluvium, highly-to-moderately-weathered ECBF and slightly weathered ECBF soil layers were defined using recommendations from Reese and Welch [51] for over consolidated stiff clay. The ultimate capacity of the p-y springs (pult) were defined based on undrained shear strength derived from CPT tip resistance based correlations [52]. The displacement at which 50% of pult is mobilised (y50) were defined based on the pile diameter and the recommended range of strain50 values for Auckland clays (0.0015-0.002) from Sa'don et al [25]. The general formula for undrained shear strength can be written as:

$$s_u = (q_c - \sigma_{v0})/N_k \quad (1)$$

where s_u = undrained shear strength, q_c = CPT tip resistance, σ_{v0} = total overburden stress and N_k = empirical cone factor, that varies between 11 and 19.

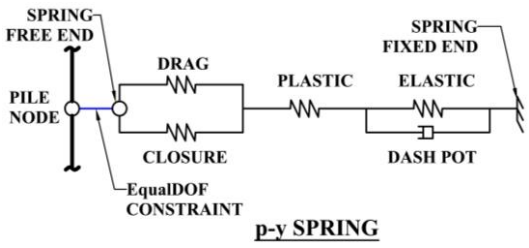

Figure 10: Characteristics of a non-linear p-y spring.

NUMERICAL RESULTS

Static Pushover Tests

The experimental and numerical load-displacement responses for each specimen are compared in Figure 11. In general, the numerical results compared well with the experimental observations for both specimens in terms of soil gapping, displacements at peak loads, and stiffness. Numerical and experimental results were similar up until S1_T3 for Specimen 1 in Figure 11 (a), with results diverging at loads greater than 100 kN. The lack of additional gap development during Tests 6-9 was also evident in the numerical results. The model for Specimen 2 in Figure 11(b) was able to capture the response up to test S2_T5. However, the numerical results for Specimen 2 did not accurately capture soil gapping following the maximum applied load during Test 5, as soil gapping was significantly underestimated by the model for Tests 6-9 (as shown in Figure 11). This may have been a result of the variability of the soil at the site, however further refinement of the model was not warranted.

To further explore the pushover response of each specimen, the variation of bending moment along the specimen height is presented in Figure 12. The location of the peak bending moment shifted downwards with an increase in the peak loading from Test 1 to Test 5 for both specimens, and varied between approximately 1-3 pile diameters below the ground surface for Specimen 1 and for Specimen 2 which is consistent with observations made by other researchers [17,29,44,53,54]. The location of peak bending moment in Specimen 1 in Figure 12 (a) shifted from a depth of 0.85 m for the 50 kN tests performed before peak loading (S1_T1 and S1_T2) to a 2.75 m depth for those tests performed after peak loading (S1_T6 and S1_T9). This is a result of gapping between the soil and pile, which influences the effective unsupported length of the integrated pile-column. A similar shift in the location of peak bending moment was observed between S1_T3 and S1_T8 and between S1_T4 and S1_T7. The peak bending moment locations for Specimen 2 in Figure 12 (b) showed a similar trend. These shifts in the bending moment profiles throughout the test sequence, and the differences between tests with similar load levels clearly demonstrates the influence of gapping around the pile and its importance in understanding foundation demands.

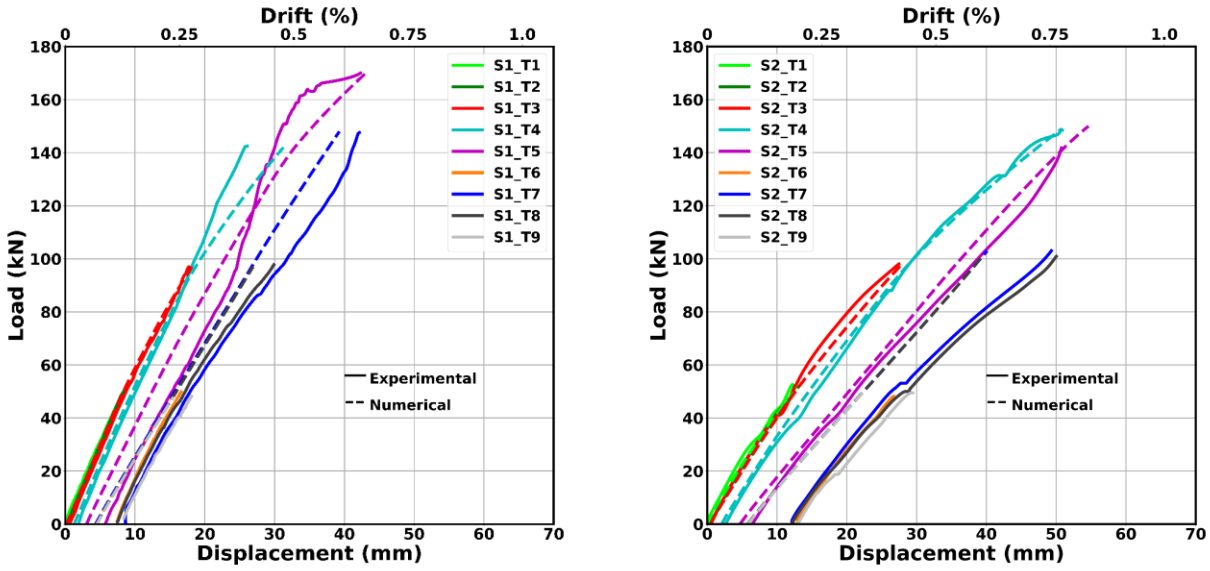

(a) **(b)**

Figure 11: Comparison of the load-displacement behaviour during static pushover loading for the field test and OpenSeesPy models for (a) Specimen 1; (b) Specimen 2.

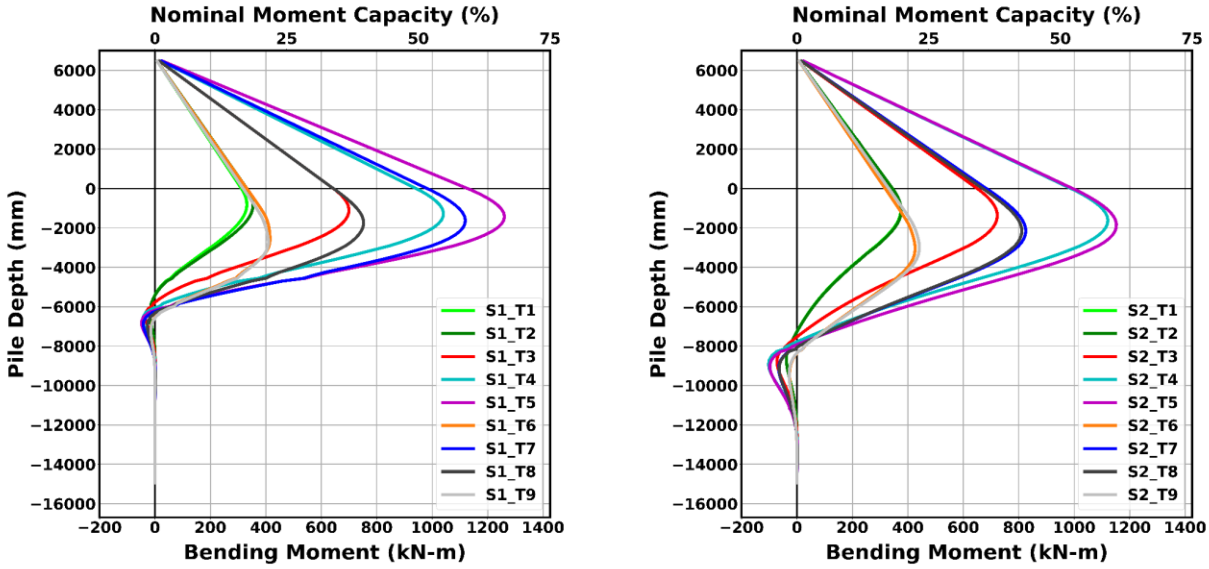

(a) **(b)**

Figure 12: Variation of the bending moment profiles for the OpenSeespy models for a) Specimen 1; b) Specimen 2.

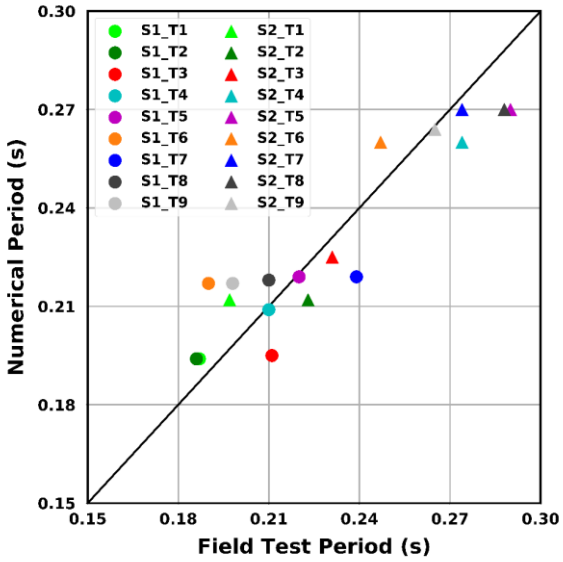

Figure 13: Comparison of natural period from field tests and the OpenSeesPy models for both specimens.

Snapback Tests

The snapback tests were used to evaluate the accuracy of the acceleration response predicted by the model. The experimental and numerical periods are shown in Figure 13 while the response histories from selected snapback tests have been plotted in Figure 14 (the full set of response histories is summarised in the electronic supplement). The natural period of the two specimens from OpenSeesPy models was estimated for each snapback test by identifying the peak in the Fast Fourier Transformation (FFT) of the time series data. In general, there is a good comparison between the experimental and numerical periods and dynamic response histories, with most of the periods from the numerical models within 10% of periods calculated from field testing. The models were able to replicate the snapback behaviour of both the specimens across all levels of loading. The model captured the acceleration response history well during the initial low level snapback tests of S1_T1 and during low level snapback test S1_T9, after the application of maximum loading in S1_T5. In both these tests the specimens have low initial acceleration and the acceleration decay was gradual throughout. The model also captured the acceleration response history well during the high level snapback tests of S1_T4 and S1_T5. In these tests the specimens had large initial accelerations with high acceleration decay due to the impact, followed by lower accelerations with gradual decay.

SENSITIVITY ANALYSIS

To evaluate the influence of key parameters on the pushover response of the integrated pile columns, a limited sensitivity analysis was conducted using Specimen 1 with the application of a 100 kN load as a reference. Specimen 1 was chosen for the sensitivity study as OpenSeesPy models were able to closely match the observed field testing response at this load level, including the lateral displacements, soil gapping, fundamental periods and acceleration time histories. For the loading range being assessed the parameters that were the focus of the sensitivity study were the initial tangent modulus of concrete, the ultimate capacity of the p-y springs (p_{ult}) and the displacement at which 50% of p_{ult} is mobilised (y_{50}). The initial tangent modulus of concrete was modified by varying the concrete compressive strength, with values 76% to 125% of the reference value. This range is perhaps much larger than the overall uncertainty expected for structural properties, however the effects of ageing could account for the upper bounds of the uncertainty range, and the lower bound provides an analogue for accounting for the cracked stiffness of the pile-column. For each soil layer p_{ult} was varied directly, while the y_{50} value was modified by varying the strain50 value. The sensitivity to both these parameters was assessed using 50% to 200% of the reference value [55].

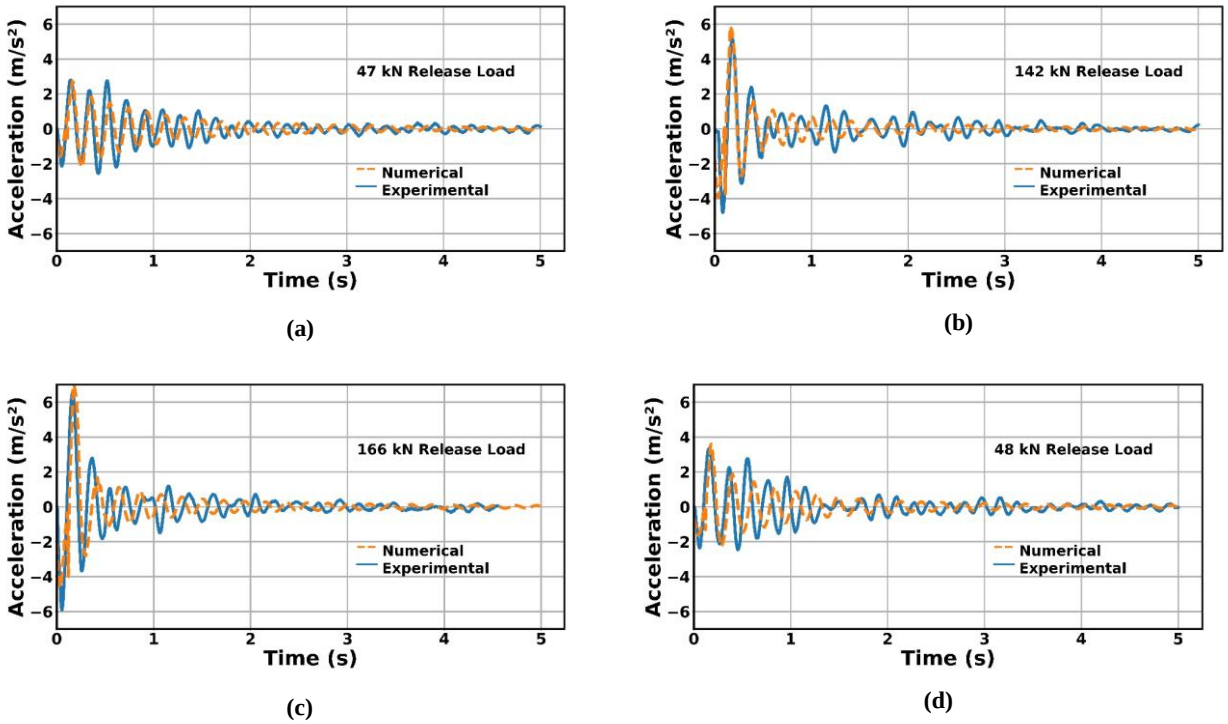

Figure 14: Comparison of the snapback acceleration response histories from field testing and OpenSeesPy models for Specimen 1 (a) S1_T1; (b) S1_T4; (c) S1_T5; (d) S1_T9.

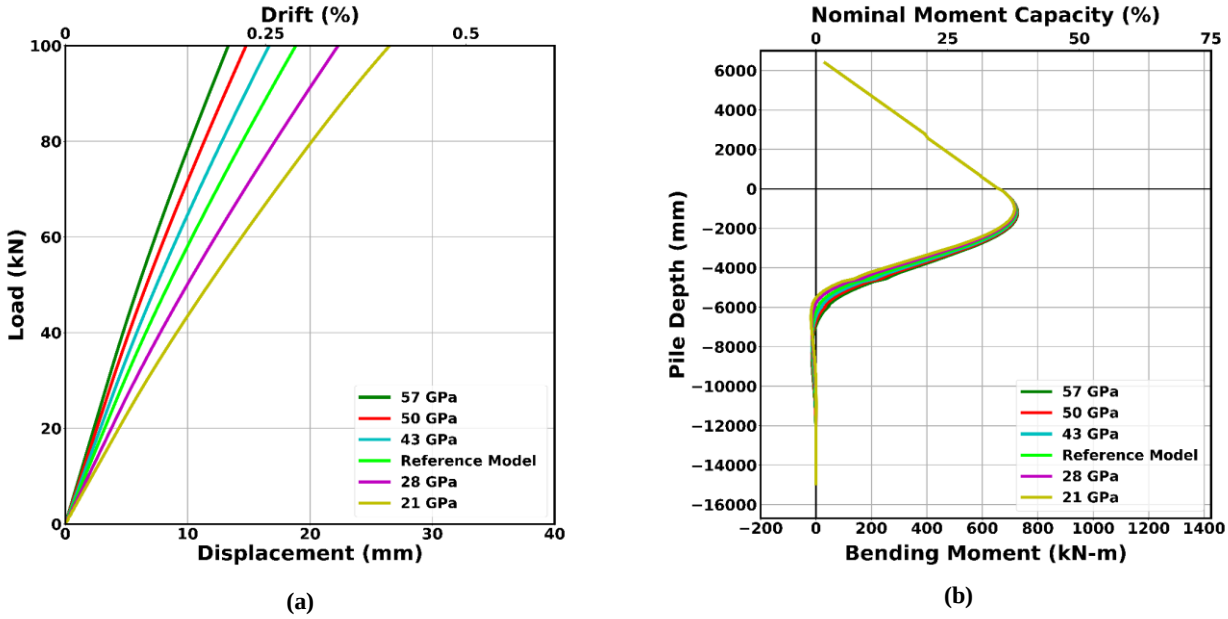

Figure 15: Effect of initial tangent modulus of concrete on (a) Specimen head displacements; (b) Peak bending moment profiles.

The influence of the initial tangent modulus of concrete on the pushover response is illustrated in Figure 15, with six different modulus values used to demonstrate the variation in response. There was a 29% reduction in secant stiffness for a 24% reduction in the initial tangent modulus, while there was a 42% increase in secant stiffness for a 25% increase in the initial tangent modulus. As the initial tangent modulus increased, the rate at which the secant stiffness of the integrated pile-column increased slowed.

At some point further increases in the initial tangent modulus will have little effect on the specimen head deflections and system period, with the behaviour of the system dictated by the soil properties. The location of the peak bending moment was not influenced by the initial tangent stiffness of the concrete as indicated in Figure 15b.

The influence of the variation of soil properties for each soil layer on the pushover response is shown in Figure 16 and Figure 17 for p_{ult} and y_{50}, respectively. In general, only the properties of the top soil layer (ground level to 4.5 m) influenced the static force-displacement response and bending moment distribution along the height, with minimal influence on response observed when the properties of the middle (4.5 m to 6 m from top of ground level) and bottom layers (6 m to pile bottom from top of ground level) were varied. Modifying p_{ult} in the top soil layer resulted in a 22% reduction in secant stiffness when the top layer p_{ult} was reduced to 50% of the reference model while there was an increase of 22% in secant stiffness when the top layer

p_{ult} was increased to 200% of the reference model. The peak bending moment location shifted 0.35 m upwards compared to the reference model when the top layer p_{ult} was increased by 200% and moved 0.55 m downwards when the top layer p_{ult} was reduced by 50%.

Similarly, there was a 10% increase in secant stiffness when the top layer y_{50} was reduced to 50% of the reference model while there was a 10% reduction in secant stiffness when the top layer y_{50} was increased to 200% of the reference model. The peak bending moment location shifted 0.1 m upwards towards the ground level from the reference peak moment location of 1 m when the top layer y_{50} was reduced to 50% of the reference model. The peak bending moment location moved 0.2 m downwards when the top layer y_{50} was increased to 200% of the reference model.

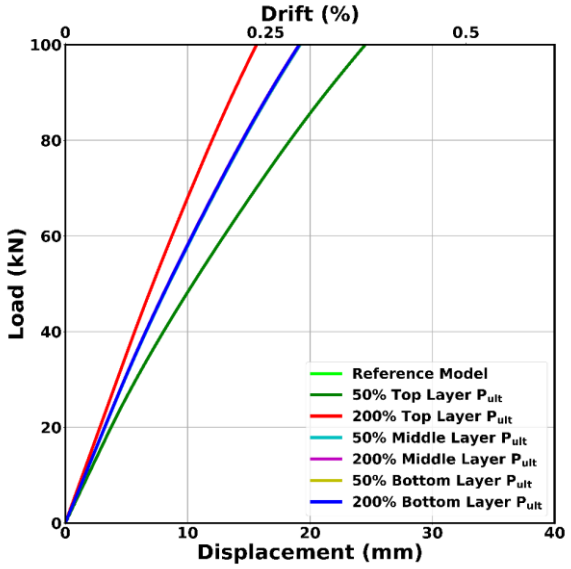

(a)

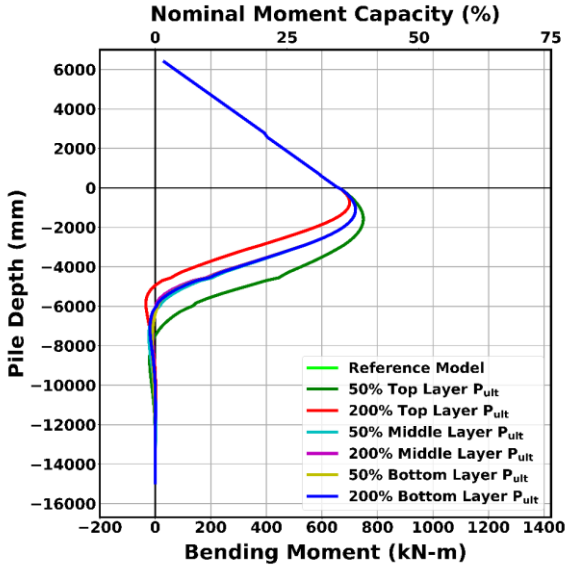

(b)

Figure 16: Effect of p_{ult} value of soil p-y springs on a) Specimen head displacements; b) Peak bending moment profile.

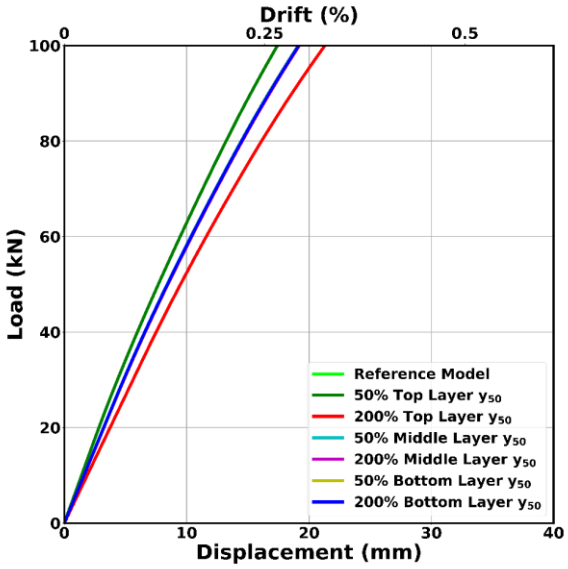

(a)

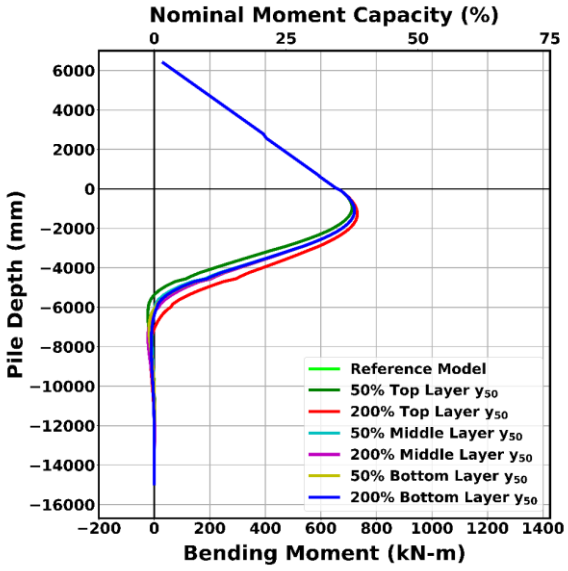

(b)

Figure 17: Effect of p_{ult} value of soil p-y springs on a) Specimen head displacements; b) Peak bending moment profile.

The combined results of the sensitivity analysis are summarised in Figure 18 with respect to the change in secant stiffness to highlight the controlling parameters. There clearly is significant sensitivity to changes in the concrete initial tangent modulus for the range considered. Only the p_{ult} and y_{50} parameters of the top soil layer influenced the response relative to the reference model, and the model remained insensitive to changes in p_{ult} and y_{50} values of the underlying soil layers. The importance of the soil strength and stiffness of the near surface soil layers on overall response are consistent with the observations made by other researchers [24,26]. The results in Figure 18 in terms of exact values are only directly applicable to Specimen 1, however the general trends related to which parameters control response would still be applicable to Specimen 2.

Figure 18: Sensitivity of the specimen secant stiffness to variation in soil layer properties and concrete modulus. The range of variation for each parameter is summarised in brackets in the vertical axis.

CONCLUSIONS

Static pushover and snapback tests were performed on two concrete integrated pile-column specimens of the Henderson Creek Bridge No. 2 to determine the static and dynamic behaviour of each specimen. The test sequence was chosen in order to capture the change in dynamic response, and variation in stiffness and damping of the specimen due to soil nonlinearity, gapping and cracking of the pile-column. The experimental results were used to validate a nonlinear model developed in OpenSeesPy, using a Nonlinear Beam on Winkler Foundation approach. Based on the field testing and modelling results, the following conclusions can be drawn:

- Loading history has a significant influence on the secant stiffness of integrated pile-columns, with reduction in secant stiffness of up to 40% observed, primarily due to soil gapping around the piles.
- Damping during the dynamic response of integrated pile-columns is influenced by a combination of mechanisms, including impact between the pile and surrounding soil and gapping. These mechanisms vary depending on the level of excitation and loading history, suggesting that constant equivalent viscous damping values should not be used when accounting for soil-foundation-structure interaction effects as part of detailed component modelling. For the wider analysis of bridges, the values suggested by NZ Transport Agency Bridge Manual for piles seems to provide a conservative estimate of the damping these components can provide.
- The existing p-y curves for clay type of soils can accurately predict the static and dynamic response of the integrated pile-columns, when appropriate soil and concrete material properties according to site conditions are provided.
- Even when the top soil layer consists of soft alluvial soils, the strength and stiffness of this layer has a significant effect on the lateral specimen head deflection, secant stiffness, period and the peak bending moment location of specimen-soil system. This reinforces the need for good characterisation of the near surface soil profile in order to capture the behaviour of the system.

ACKNOWLEDGEMENTS

Authors would like to acknowledge the financial support of the New Zealand Transport Agency and QuakeCoRE, a New Zealand centre of research excellence in earthquake resilience. We acknowledge the on-site logistical support of Fulton Hogan Ltd and John Wood for his role in facilitating the start of this project. This is QuakeCoRE publication number 0596.

REFERENCES

1 Novak M (1991). “Piles under dynamic loads”. *2nd International Conference on Recent Advances on Geotechnical Earthquake Engineering and Soil Dynamics*, **3**: (2433–2456). https://scholarsmine.mst.edu/icrageesd/02icrageesd/session14/12/

2 Paulay T and Priestley MN (1992). *Seismic Design of Reinforced Concrete and Masonry Buildings*. John Wiley & Sons, Inc.

3 Mylonakis G, Nikolaou A and Gazetas G (1997). “Soil–pile–bridge seismic interaction: Kinematic and inertial effects. Part I: Soft soil”. *Earthquake Engineering and Structural Dynamics*, **26**(3): 337–359. https://doi.org/10.1002/(SICI)1096-9845(199703)26:3<337::AID-EQE646>3.0.CO;2-D

4 Gazetas G and Mylonakis G (1998). “Seismic soil–structure interaction: New evidence and emerging issues, emerging issues”. *Geotechnical Earthquake Engineering and Soil Dynamics III*, **46**(13): 1119–1174. https://cedb.asce.org/CEDBsearch/record.jsp?dockey=0112765

5 Mylonakis G and Gazetas G (2000). “Seismic soil-structure interaction: beneficial or detrimental?”. *Journal of Earthquake Engineering*, **4**(3): 277–301. https://doi.org/10.1080/13632460009350372

6 Matlock H (1970). “Correlations for design of laterally loaded piles in soft clay”. *Offshore Technology in Civil Engineering’s Hall of Fame Papers from the Early Years*, 1970-April: 77–94. https://cedb.asce.org/CEDBsearch/record.jsp?dockey=0279673

7 Kramer SL (1991). “*Behavior of Piles in Full-Scale, Field Lateral Loading Tests*”. Springfield, VA.

8 Rollins KM, Peterson KT and Weaver TJ (1998). “Lateral load behavior of full-scale pile group in clay”. *Journal of Geotechnical and Geoenvironmental Engineering*, **124**(6): 468–478. https://doi.org/10.1061/(ASCE)1090-0241(1998)124:6(468)

9 Gerber TM and Rollins KM (2008). “Cyclic PY curves for a pile in cohesive soil”. *Geotechnical Earthquake Engineering and Soil Dynamics*, IV: 1–10. https://doi.org/10.1061/40975(318)139

10 Sritharan S, Suleiman MT and White DJ (2007). “Effects of seasonal freezing on bridge column–foundation–soil interaction and their implications”. *Earthquake Spectra*, **23**(1): 199–222. https://doi.org/10.1193/1.2423071

11 Sadon NBM (2012). “*Full-Scale Static and Dynamic Lateral Loading of a Single Pile*”. PhD Dissertation, Department of Civil and Environmental Engineering, University of Auckland, Auckland, NZ. https://researchspace.auckland.ac.nz/bitstream/handle/2292/13100/whole.pdf?sequence=2&isAllowed=y

12 Chik ZH, Abbas JM, Taha MR and Shafiqu QSM (2009). “Lateral behavior of single pile in cohesionless soil subjected to both vertical and horizontal loads”. *European Journal of Scientific Research*, **29**(2): 194–205. https://www.researchgate.net/publication/255588632_Late

ral Behavior of Single Pile in Cohesionless Soil Subjected to Both Vertical and Horizontal Loads

13 Nasr AM (2014). "Experimental and theoretical studies of laterally loaded finned piles in sand". *Canadian Geotechnical Journal*, **51**(4): 381–393. https://doi.org/10.1139/cgj-2013-0012

14 Reddy MK and Ayothiraman R (2015). "Experimental studies on behavior of single pile under combined uplift and lateral loading". *Journal of Geotechnical and Geoenvironmental Engineering*, **141**(7). https://doi.org/10.1061/(ASCE)GT.1943-5606.0001314

15 Khari M, Kassim KA and Alimohammadi P (2015). "Response of single and grouped pile subjected to lateral load in cohesionless soil". *Applied Mechanics and Materials*, **773**: 1397–1401. https://doi.org/10.4028/www.scientific.net/AMM.773-774.1397

16 Abadie CN (2015). "*Cyclic Lateral Loading of Monopile Foundations in Cohesionless Soils*". PhD Dissertation, Department of Civil Engineering, University of Oxford. https://ora.ox.ac.uk/objects/uuid:b3002ca4-742d-4b08-836f-1c15eafb7156

17 Aguirre DA, Kowalsky MJ, Nau JM, Gabr M and Lucier G (2018). "Seismic performance of reinforced concrete filled steel tube drilled shafts with inground plastic hinges". *Engineering Structures*, **165**: 106–119. https://doi.org/10.1016/j.engstruct.2018.03.034

18 Lalicata LM, Desideri A, Casini F and Thorel L (2019). "Experimental observation on laterally loaded pile in unsaturated silty soil". *Canadian Geotechnical Journal*, **56**(11): 1545–1556. https://doi.org/10.1139/cgj-2018-0322

19 Rollins K, Olsen R, Egbert J, Olsen K, Jensen D and Garrett B (2003). "*Response, Analysis, and Design of Pile Groups Subjected to Static and Dynamic Lateral Loads*". UT-03.03, Utah Department of Transportation Research Division, Utah. https://rosap.ntl.bts.gov/view/dot/27636

20 Snyder JL (2004). "*Full-Scale Lateral-Load Tests of a 3x5 Pile Group in Soft Clays and Silts*". Master Thesis, Department of Civil and Environmental Engineering, Brigham Young University, UK. https://scholarsarchive.byu.edu/cgi/viewcontent.cgi?article=1122&context=etd

21 Stewart JP, Taciroglu E, Wallace JW, Ahlberg ER, Lemnitzer A, Rha C and Salamanca A (2007). "*Full Scale Cyclic Large Deflection Testing of Foundation Support Systems for Highway Bridges . Part I : Drilled Shaft Foundations*".UCLA-SGEl 2007/01, UCLA, Los Angeles, 228 pp. https://escholarship.org/uc/item/5mt9q0m6

22 Blaney GW and O'Neill MW (1989). "Dynamic lateral response of a pile group in clay". *ASTM Geotechnical Testing Journal*, **12**(1): 22–29.

23 Crouse CB, Kramer SL, Mitchell R and Hushmand B (1993). "Dynamic tests of pipe pile in saturated peat". *Journal of Geotechnical Engineering*, **119**(10): 1550–1567. https://doi.org/10.1061/(ASCE)0733-9410(1993)119:10(1550)

24 Boominathan A and Ayothiraman R (2006). "Dynamic response of laterally loaded piles in clay". *Proceedings of Institution of Civil Engineers*, **159**(3): 233–241. https://doi.org/10.1680/geng.2006.159.3.233

25 Sa'don NM, Pender M J, Karim AA and Orense R (2014). "Pile head cyclic lateral loading of single pile". *Geotechnical and Geological Engineering*, **32**(4): 1053-1064. httpa://doi.org/10.1007/s10706-014-9780-5

26 Fleming BJ, Sritharan S, Miller GA and Muraleetharan KK (2016). "Full-scale seismic testing of piles in improved and unimproved soft clay". *Earthquake Spectra*, **32**(1): 239-265. https://doi.org/10.1193/012714EQS018M

27 Scott RF, Tsai CF, Steussy D and Ting JM (1982). "Full-scale dynamic lateral pile tests". *Proceedings of the Fourteenth Offshore Technology Conference*, pp. 435–439.

28 Ting JM (1987). "Full-scale cyclic dynamic lateral pile responses". *ASCE Journal of Geotechnical Engineering*, **113**(1): 30–45. https://doi.org/10.1061/(ASCE)0733-9410(1987)113:1(30)

29 Chai YH and Hutchinson TC (2002). "Flexural strength and ductility of extended pile-shafts. II: Experimental study". *Journal of Structural Engineering*, **128**(5): 595–602. https://doi.org/10.1061/(ASCE)0733-9445(2002)128:5(595)

30 Boulanger RW, Kutter BL, Brandenberg SJ, Singh P and Chang D (2003). "*Pile Foundations in Liquefied and Laterally Spreading Ground during Earthquakes: Centrifuge Experiments and Analyses*". Research Report Centre for Geotechnical Modelling, University of California Davis, 205. https://faculty.engineering.ucdavis.edu/boulanger/wp-content/uploads/sites/71/2014/09/Boulanger_et_al_CGM03_01.pdf

31 Chang BJ and Hutchinson TC (2013). "Experimental investigation of plastic demands in piles embedded in multi-layered liquefiable soils". *Soil Dynamics and Earthquake Engineering*, **49**: 146–156. https://doi.org/10.1016/j.soildyn.2013.01.012

32 Boulanger RW, Curras CJ, Kutter BL, Wilson DW and Abghari A (1999). "Seismic soil-pile-structure interaction experiments and analyses". *Journal of Geotechnical and Geoenvironmental Engineering*, **125**(9): 750–759. https://doi.org/10.1061/(ASCE)1090-0241(1999)125:9(750)

33 Brown DA (1994). "Evaluation of static capacity of deep foundations from Statnamic testing". *Geotechnical Testing Journal*, **17**(4): 403–414. https://doi.org/10.1520/GTJ10301J

34 El Naggar MH(1998). "Interpretation of lateral statnamic load test results". *Geotechnical Testing Journal*, **21**(3): 169–179. https://doi.org/10.1520/GTJ10890J

35 Brown DA (2007). "Rapid lateral load testing of deep foundations". *DFI Journal-The Journal of Deep Foundation Institute*, **1**(1): 54–62. https://doi.org/10.1179/dfi.2007.005

36 Brown MJ, Hyde AFL and Anderson WF (2006). "Analysis of a rapid load test on an instrumented bored pile in clay". *Geotechnique*, **56**(9): 627–638. https://doi.org/10.1680/geot.2006.56.9.627

37 Brown MJ and Hyde AFL (2006). "Some observations on statnamic pile testing". *Proceedings of Institute of Civil Engineering and Geotechnical Engineering*, **159**(4): 269–273. https://doi.org/10.1680/geng.2006.159.4.269

38 Tobita T, Kang GC, Iai S and Rollins KM (2008). "Analysis of statnamic behavior of full-scale pile group in soft clays and silts". *Geotechnical Earthquake Engineering and Soil Dynamics*, IV: 1–10. https://doi.org/10.1061/40975(318)138

39 Brown DA, O'Neill MW, Hoit M, McVay M, El Naggar MH and Chakraborthy S (2001). "*Static and Dynamic Lateral Loading of Pile Groups*". NCHRP 24-9, Highway Research Center, Alabama, 172 pp. https://www.eng.auburn.edu/files/centers/hrc/NCHRP-24-9.pdf

40 Bowles SI (2005). "*Statnamic Lateral Load Testing and Analysis of a Drilled Shaft in Liquefied Sand*". Master

Thesis, Department of Civil and Environmental Engineering, Brigham Young University, UK. https://scholarsarchive.byu.edu/cgi/viewcontent.cgi?article=1722&context=etd

41 Broderick RD (2007). "*Statnamic Lateral Loading Testing of Full-Scale 15 and 9 Group Piles in Clay*". Master Thesis, Department of Civil and Environmental Engineering, Brigham Young University, UK. https://scholarsarchive.byu.edu/cgi/viewcontent.cgi?article=1860&context=etd

42 Wang S, Kutter BL, Chacko MJ, Wilson DW, Boulanger RW and Abghari A (1998). "Nonlinear seismic soil-pile structure interaction". *Earthquake Spectra*, **14**(2): 377–396. https://doi.org/10.1193/1.1586006

43 Zhu M, McKenna F and Scott MH (2018). "OpenSeesPy: *Python Library for the OpenSees Finite Element Framework*". SoftwareX, Vol. 7, pp. 6–11. https://doi.org/10.1016/j.softx.2017.10.009

44 Wood JH and Phillips M (1989). "*Lateral Stiffness of Bridge Pile Foundations: Load Tests on Maitai River Bridge*". St 88/1, National Roads Board, NZ.

45 Marder KJ, Motter CJ, Elwood KJ and Clifton GC (2018). "Effects of variation in loading protocol on the strength and deformation capacity of ductile reinforced concrete beams". *Earthquake Engineering and Structural Dynamics*, **47**(11): 2195–2213. https://doi.org/10.1002/eqe.3064.

46 Chopra AK (1995). *Dynamics of Structures: Theory and Applications to Earthquake Engineering*". ISBN 10: 0-13-285803-7, Prentice Hall. Inc. 980 pp.

47 New Zeland Transport Agency (2014). *New Zealand Transport Agency Bridge Manual*. New Zeland Transport Agency, Wellington, NZ, 294 pp. https://www.nzta.govt.nz/assets/resources/bridge-manual/docs-3rd-edition/Bridge-manual-pdf-complete-v3.3.pdf

48 NZSEE (2006). "*Assessment and Improvement of the Structural Performance of Buildings in Earthquakes: Prioritisation, Initial Evaluation, Detailed Assessment, Improvement Measures: Recommendations of a NZSEE Study Group on Earthquake Risk Buildings*". New Zealand Society for Earthquake Engineering, Wellington, NZ, 368 pp. https://www.nzsee.org.nz/db/PUBS/2006AISBEGUIDELINES_Corr_06a.pdf

49 Mander JB, Priestley MJ and Park R (1988). "Theoretical stress-strain model for confined concrete". *Journal of Structural Engineering*, **114**(8): 1804–1826. https://doi.org/10.1061/(ASCE)0733-9445(1988)114:8(1804)

50 Davies TG and Budhu M (1986). "Non-linear analysis of laterally loaded piles in heavily overconsolidated clays". *Géotechnique*, **36**(4): 527–538. https://doi.org/10.1680/geot.1986.36.4.527

51 Reese LC, Cox WR and Koop FD (1975). "Field testing and analysis of laterally loaded piles om stiff clay". *Offshore Technolology Conference*, OTC, Houston, USA. https://doi.org/10.4043/2312-MS

52 Lunne T, Robertson PK and Powell J (1997). *Cone Penetration Testing in Geotechnical Practice*. Blackie Academic and Professional. Chapman and Hall, NY, USA. https://doi.org/10.1007/s11204-010-9072

53 Allotey N and El Naggar MH (2008). "Generalized dynamic Winkler model for nonlinear soil–structure interaction analysis". *Canadian Geotechnical Journal*, **45**(4): 560–573. https://doi.org/10.1139/T07-106

54 Allotey N and El Naggar MH (2008). "A numerical study into lateral cyclic nonlinear soil–pile response". *Canadian Geotechnical Journal*, **45**(9): 1268–1281. https://doi.org/10.1139/T08-050

55 BSSC US (1997). "*NEHRP Guidelines for the Seismic Rehabilitation of Buildings*". FEMA 273, Federal Emergency Manalgement Agency, Washington, DC, 435 pp. https://www.conservationtech.com/FEMA-publications/FEMA273-1997.pdf

APPENDIX

This supplement provides the comparison between the experimental and numerical response histories of both Specimen 1 and Specimen 2 in all the snapback tests performed.

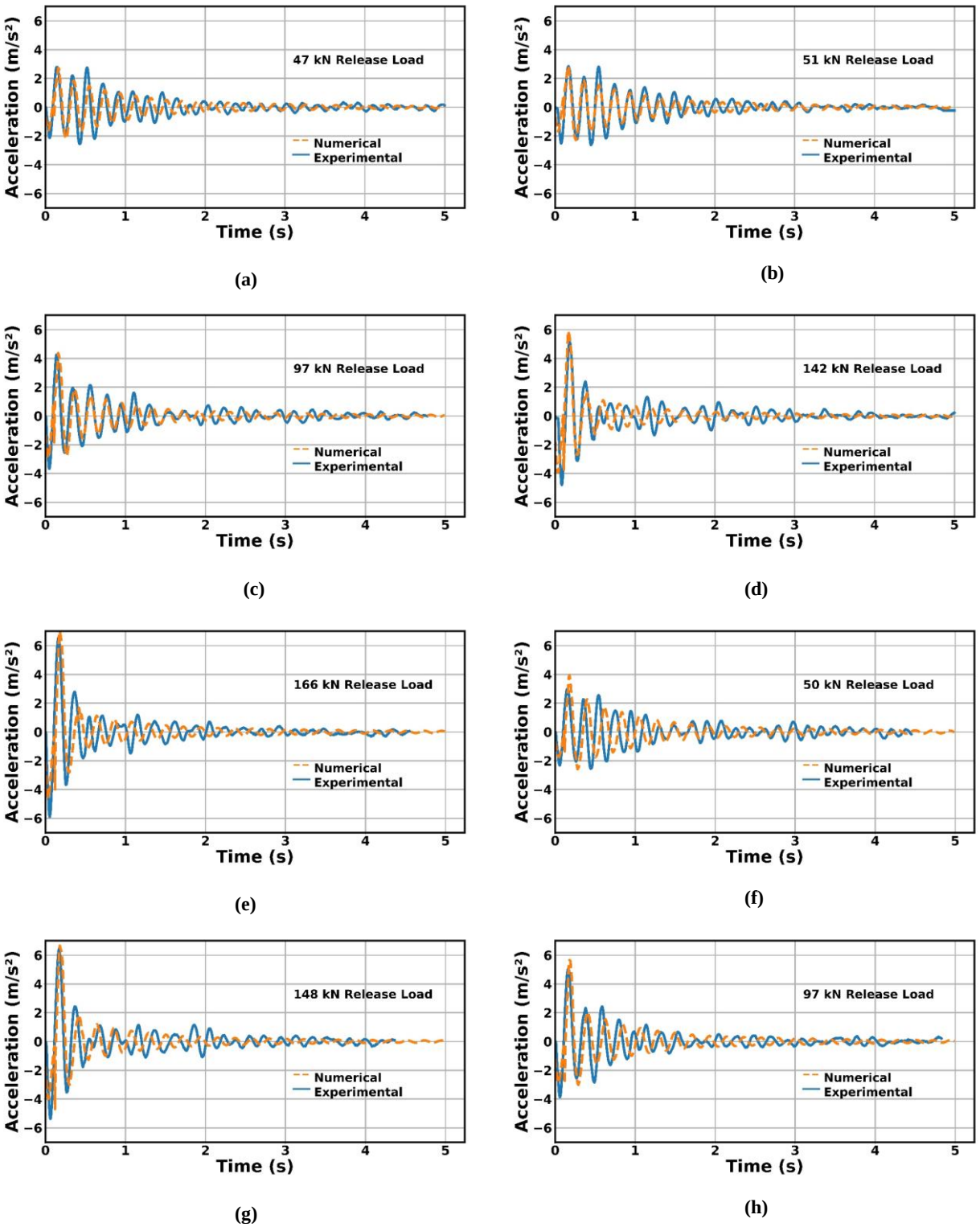

Figure A.19: Comparison of the snapback acceleration response histories from field testing and OpenSeesPy models for Specimen 1 (a) S1_T1; (b) S1_T2; (c) S1_T3; (d) S1_T4; (e) S1_T5; (f) S1_T6; (g) S1_T7; (h) S1_T8; (i) S1_T9 (cont.).

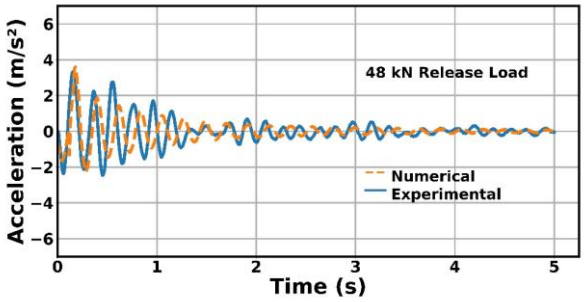

(i)

Figure A.20: Comparison of the snapback acceleration response histories from field testing and OpenSeesPy models for Specimen 1 (a) S1_T1; (b) S1_T2; (c) S1_T3; (d) S1_T4; (e) S1_T5; (f) S1_T6; (g) S1_T7; (h) S1_T8; (i) S1_T9.

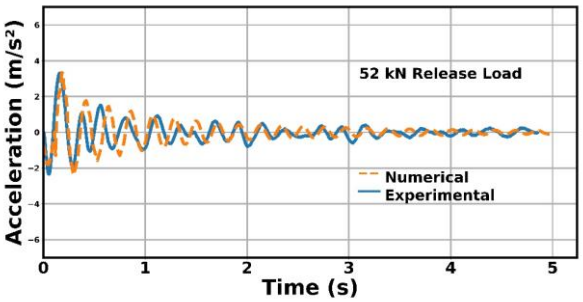

(a)

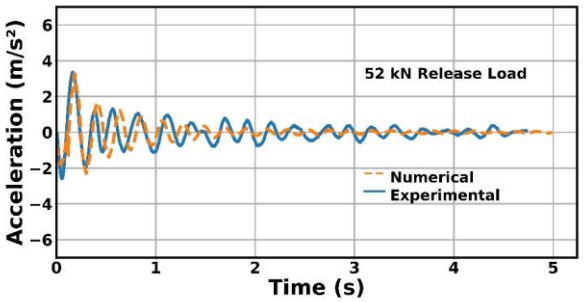

(b)

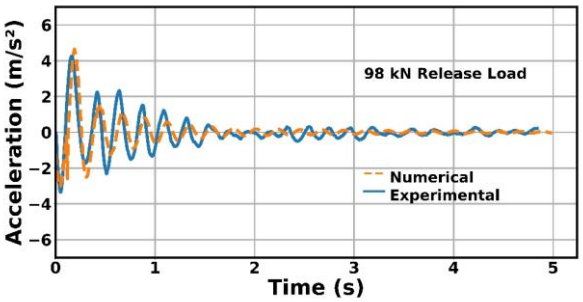

(c)

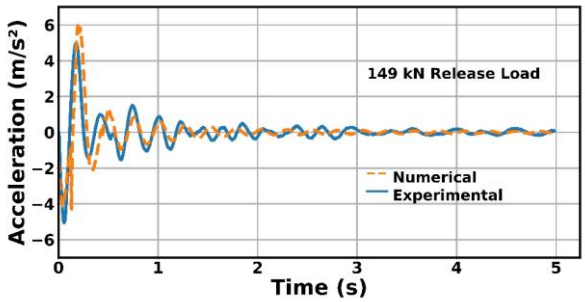

(d)

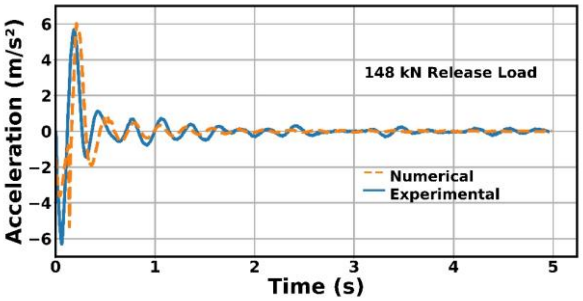

(e)

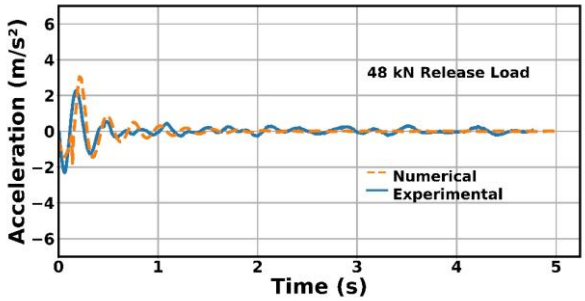

(f)

Figure A.21: Comparison of the snapback acceleration response histories from field testing and OpenSeesPy models for Specimen 2 (a) S2_T1; (b) S2_T2; (c) S2_T3; (d) S2_T4; (e) S2_T5; (f) S2_T6; (g) S2_T7; (h) S2_T8; (i) S2_T9 (cont.).

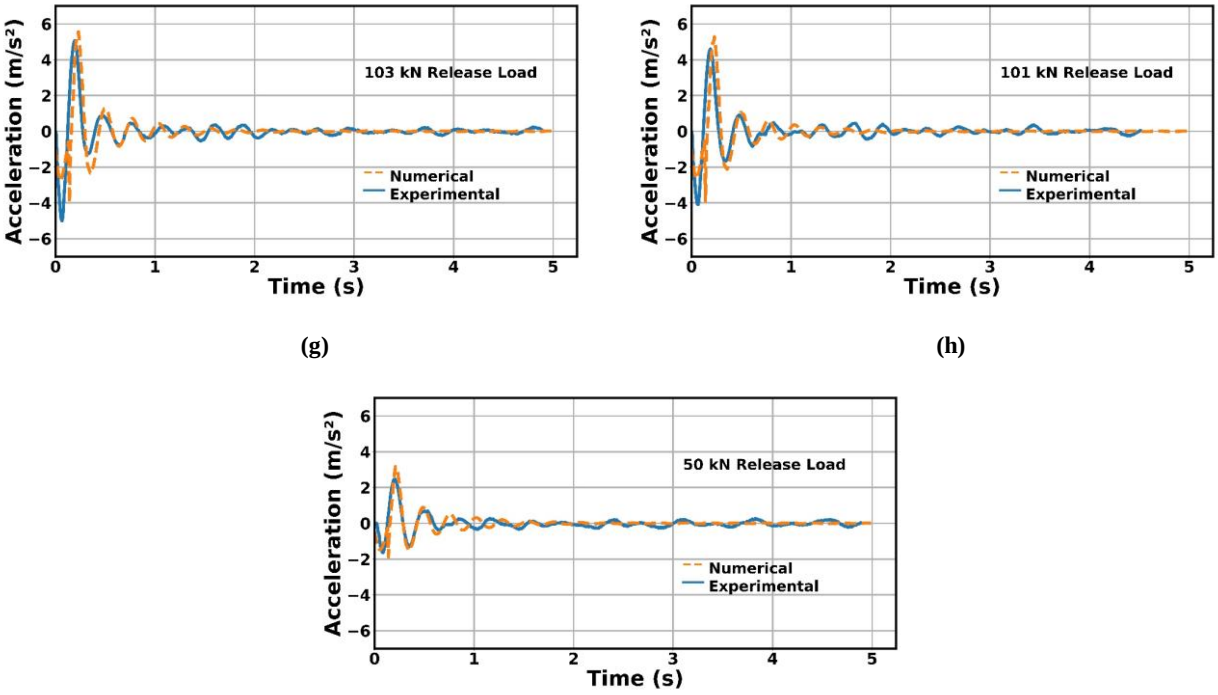

(g) **(h)**

(i)

Figure A.22: Comparison of the snapback acceleration response histories from field testing and OpenSeesPy models for Specimen 2 (a) S2_T1; (b) S2_T2; (c) S2_T3; (d) S2_T4; (e) S2_T5; (f) S2_T6; (g) S2_T7; (h) S2_T8; (i) S2_T9.